RSC Advances

PAPER

View Article Online
View Journal | View Issue

Cite this: *RSC Adv.*, 2022, **12**, 3097

Rational fabrication of a new ionic imprinted carboxymethyl chitosan-based sponge for efficient selective adsorption of Gd(III)

Enli Liu,[ab] Junyou Shi,*[ab] Xue Lin,[b] Wenbiao Xu,[b] Liyun Feng[b] and Yuanzhi Hong*[b]

The selective recovery of Gd(III) from wastewater is very meaningful for the prospective development of economics and the environment. To overcome disadvantages of poor adsorption capacity, low selectivity and complex preparation process in conventional adsorbents, herein a new ionic imprinted carboxymethyl chitosan (CMC) sponge functionalized by hyperbranched polyethyleneimine (PEI) with a 3D network structure (PEI-CMC-IIS) was successfully prepared and applied in the selective adsorption of Gd(III). The PEI-CMC-IIS is endowed with lots of amino groups due to the combination of biomass CMC with highly branched PEI, which is helpful for the adsorption of Gd(III). The imprinting sites are located at the surface of channels in PEI-CMC-IIS, which can achieve the adsorption specificity to Gd(III) and improve adsorption capacity. It is found that the maximum adsorption capacity of PEI-CMC-IIS is 38.64 mg g^{-1} at pH = 7. Meanwhile, the selectivity tests suggest that the PEI-CMC-IIS presents preferential adsorption for Gd(III) with a distribution coefficient of 437.5 mL g^{-1}. Furthermore, the PEI-CMC-IIS displays excellent reusing and regeneration ability. Our findings will bring about potential application in fabrication of other high-efficiency adsorbents for selective adsorption of Gd(III).

Received 5th November 2021
Accepted 3rd January 2022

DOI: 10.1039/d1ra08115b

rsc.li/rsc-advances

1. Introduction

The widespread application of rare earth metals (REMs) owing to their excellent optical, magnetic, and electronic properties drastically exacerbates the release of REM ions into the aquatic environment, which is potentially dangerous for the health of humans and animals.[1–3] The free gadolinium ion [Gd(III)] accumulated in water is extremely poisonous, and may destroy the human immune and respiratory system.[4–6] Thus, development of an effective avenue for separation and recovery of Gd(III) from wastewater plays an increasingly significant role in advanced applications. Up to now, among numerous techniques proposed, the adsorption strategy stands out because of its handiness and high efficiency. Such adsorbents as cellulose-based materials,[7,8] pseudomonas fluorescens cells[9] and silica-based materials[10] are applied to remove metal ions from water. Unfortunately, these adsorbents are generally formed in powder or granular, which is difficult to regenerate, therefore the treatment process is very awkward. To this end, it is meaningful to develop an ingenious adsorbent with high adsorption performance and easy separation from solution.

Carboxymethyl chitosan (CMC) sponge obtained by the modification of chitosan and lyophilization, is an important derivative in the area of adsorption.[11–13] On the one hand, the CMC sponge is endowed with the unique 3D network structure and excellent elasticity, which is helpful for its easy recyclability. On the other hand, the CMC sponge contains a large number of highly hydrophilic functional groups (–NH_2, –OH, –COOH), which can strongly chelate with Gd(III).[14,15] That is to say, these outstanding advantages make CMC sponge potential value in the removal of Gd(III) from water. Nevertheless, it should be pointed that the low adsorption capacity is still an unresolved problem for CMC sponge. Therefore, it is necessary to chemically modify the CMC sponge and introduce more reactive groups into its surface for improving its adsorption performance.

Polyethyleneimine (PEI) has highly branched structure and abundant amine groups, which is conductive to its superior chelation ability with metal ions.[16] So, PEI is often used to modify some insoluble substances for improving their adsorption capacities, which are proved as available achievements.[17–19] According to the hard and soft acids and bases theory (HSAB), Gd(III) as hard Lewis acid displays the strong binding tendency to N atom in functional groups of PEI. From this prospect, chemical modifying the CMC sponge by PEI is expected to acquire a new adsorbent with high adsorption capacity, stable regeneration and easy separation. However, Gd(III) commonly co-exists with other REMs ions in practical aquatic

[a]*School of Agricultural Engineering and Food Science, Shandong University of Technology, Zibo 255000, People's Republic of China. E-mail: bhsjy64@163.com*
[b]*School of Materials Science and Engineering, Beihua University, Jilin 132013, People's Republic of China. E-mail: bhhyz93@163.com*

environment, such as NdFeB permanent magnet/magnetic refrigeration wastewater.[20] Moreover, the similarity in physicochemical properties among REMs ions hinders the obtainment of high-purity Gd(III). As a result, designing a high-efficiency adsorbent that can realize the selective removal of Gd(III) from water is extremely necessary.

To resolve the poor selectivity of adsorbents, ion imprinted technology (IIT) is often used to prepare new ion imprinted polymers (IIP) that can selectively adsorb metal ions due to the special ability to recognize some ion in terms of ionic geometry.[21–23] In general, template ion and functional polymer exert copolymerization in the presence of crosslinker. After removing template ion, cavities that are only complementary with template ion in size will form in IIP, which can selectively rebind template ion. In this context, combining above mentioned CMC sponge functionalized by PEI with IIT to prepare Gd(III) imprinted porous polymer is anticipant to obtain an effective adsorbent, where imprinting sites will be located at the surface of channels, facilitating the diffusion of Gd(III) to reactive sites and achieving selective adsorption of Gd(III). As far as we know, this related ideal research and experiment is unprecedented.

In this work, for the first time, a new Gd(III) imprinted PEI functionalized CMC sponge (PEI-CMC-IIS) with 3D network structure was successfully prepared for effectively selective adsorption of Gd(III). The goals of this study are following: (a) to characterize the PEI-CMC-IIS, non-imprinted PEI functionalized CMC sponge (PEI-CMC-NIIS), and imprinted CMC sponge without modification (CMC-IIS) *via* various physicochemical techniques; (b) to explore the effects of solution pH, contact time and initial Gd(III) concentration on Gd(III) adsorption; (c) to investigate the adsorption kinetics, adsorption equilibrium, adsorption selectivity and reusability of PEI-CMC-IIS; (d) to analyze Gd(III) adsorption mechanism of PEI-CMC-IIS. Consequently, the PEI-CMC-IIS promises huge value in the application of water treatment due to its comparable adsorption capacity, high selectivity, easy separation and stable recyclability towards adsorption of Gd(III) from water.

2. Experimental section

2.1. Reagents

Carboxymethyl chitosan (CMC, substitution degree ≥ 80%), branched polyethylenimine (PEI, M_w = 1.8 kDa and 25 kDa), 1-ethyl-3-[3-dimethylaminopropyl] carbodiimide hydrochloride (EDC, 98.5%) and *N*-hydroxyl succinimide (NHS, 98%) were purchased from McLean Chemical Reagent Co. Ltd. $GdCl_3 \cdot 6H_2O$ was prepared by the dissolution of Gd_2O_3 in 0.1 M hydrochloric acid (HCl). Gd_2O_3 (99.9%) and 50% glutaraldehyde (GA) were provided by Aladdin Company in Shanghai, China. Absolute ethanol, acetic acid, HCl and sodium hydroxide were all of analytical reagent grade and came from Sinopharm Chemical Reagent Co. Ltd. in Shanghai, China. Ultrapure water (UPT-A, Shenfen Analytical Instrument Co. Ltd. in Shanghai, China) with a resistivity of 18.2 MΩ cm was used in all experiments.

2.2. Preparation of adsorbents

2.2.1. Synthesis of PEI functionalized CMC. The PEI functionalized CMC was synthesized *via* amination reaction between carboxyl groups of CMC and amine groups of PEI as starting materials.[24] Firstly, 1 g of CMC was dissolved in 70 mL of ultrapure water to obtain the yellowish solution. Then, 2 g of EDC and 2 g of NHS were successively added into above solution. The pH of solution was adjusted to 5–6 and measured by PHS-3C (INESA in Shanghai, China), the solution was kept stirring for 2 hours to activate carboxyl groups on CMC. Subsequently, 3 g of branched PEI 1800 was added into above solution and the pH was adjusted to 7–8, the solution was further kept stirring for 24 hours at room temperature. Finally, the obtained solution was dialyzed against ultrapure water for 2 days to remove the unreacted EDC and NHS.

2.2.2. Fabrication of PEI-CMC-IIS. The PEI-CMC-IIS was fabricated by a simple polymerization-lyophilization method. In detail, 2 g of $GdCl_3 \cdot 6H_2O$ was dissolved in PEI functionalized CMC solution and stirred with electric mixer for 3 hours. Then, 40 mL of 5% (v/v) glutaraldehyde (GA) solution was added dropwise and stirred with electric mixer for 30 minutes at 25 °C. The obtained solution was further treated by ultrasonic to eliminate bubbles, following lyophilized to obtain sponge. Subsequently, the sponge was immersed in 1 M HCl solution for 12 hours to remove template Gd(III). Finally, the sponge went through repeated wash with ultrapure water and immersion in 1 M NaOH solution then wash-lyophilization again to obtain the PEI-CMC-IIS. The overall syntheses strategy is presented in Fig. 1. The same route was also applied to synthesize the PEI-CMC-NIIS without template Gd(III) and CMC-IIS without functionalization of CMC, respectively.

2.3. Characterization of adsorbents

The morphology of PEI-CMC-IIS, PEI-CMC-NIIS and CMC-IIS adsorbents were characterized by field-emission scanning electron microscope (SEM). The surface area and pore size distribution of PEI-CMC-IIS, PEI-CMC-NIIS and CMC-IIS adsorbents were analyzed by nitrogen (N_2) adsorption–desorption isotherms. The functional groups and element contents of PEI-CMC-IIS, PEI-CMC-NIIS and CMC-IIS adsorbents were carried out by Fourier transform infrared spectra (FT-IR) and element analysis (EA), respectively. The thermal stability of PEI-CMC-IIS, PEI-CMC-NIIS and CMC-IIS adsorbents were determined by thermogravimetric (TG) analysis. The involvement of PEI-CMC-IIS functionality with Gd(III) was studied by X-ray photoelectron spectroscopy (XPS). The concentration of supernatant after adsorption process was measured by a PerkinElmer 3000 DVICP-AES apparatus (ICP-AES).

2.4. Adsorption assays

The batch adsorption experiments of Gd(III) on different materials were carried out at 25 °C by immersing a certain amount of adsorbent into some concentration of Gd(III) solutions. The pH tests, adsorption kinetics and adsorption isotherms experiments were repeated three times. The solution of Gd(III), Nd(III),

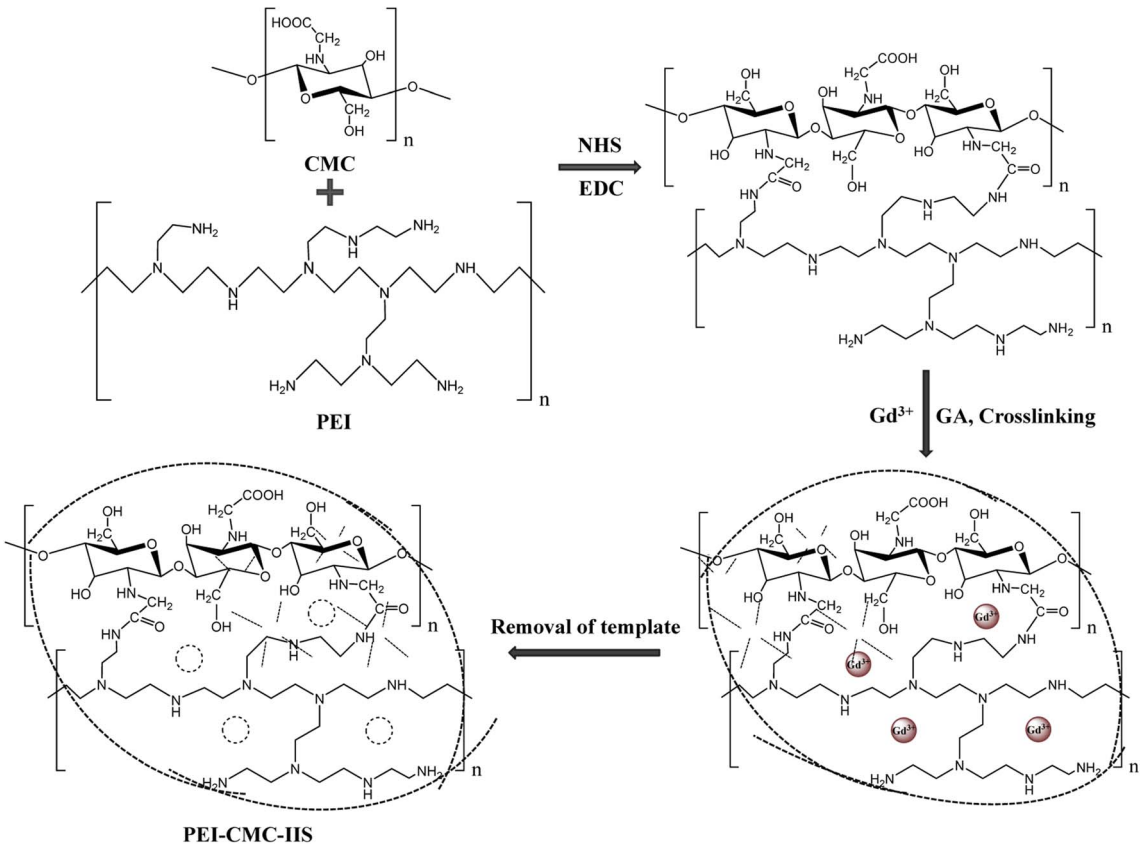

Fig. 1 Schematic illustration of the synthetical processes of PEI-CMC-IIS adsorbent.

Pr(III), Tb(III) and Fe(III) was prepared by diluting standard solution of single element solution, respectively. The adsorption capacity Q_t (mg g^{-1}) was calculated by the following equation:

$$Q_{t(e)} = \frac{(C_0 - C_{t(e)})V}{M} \quad (1)$$

where C_0 and $C_{t(e)}$ (mg L^{-1}) are the initial and final metal ion concentration in solution, respectively. V (L) and M (g) denote the volume of solution and the mass of adsorbent, respectively.

2.4.1. pH test. 10 mg of PEI-CMC-IIS, PEI-CMC-NIIS and CMC-IIS was separately immersed in Gd(III) solution (10 mL, 50 mg L^{-1}) at different pH (2 to 7) for 12 hours. The pH of Gd(III) solution was adjusted by 0.1 M of NaOH and HCl. The imprinting factor (IF) reflecting separation ability of the IIP was calculated according to the ratio of Gd(III) adsorption capacity of PEI-CMC-IIS over that of PEI-CMC-NIIS.

2.4.2. Adsorption kinetics. 10 mg of PEI-CMC-IIS, PEI-CMC-NIIS and CMC-IIS was separately immersed in Gd(III) solution (10 mL, 50 mg L^{-1}, pH = 7). The ICP-AES was used to determine the concentration of supernatant collected under different contact time (5, 15, 30, 60, 90, 180, 360 and 720 minutes), respectively.

2.4.3. Adsorption isotherms. 10 mg of PEI-CMC-IIS, PEI-CMC-NIIS and CMC-IIS was separately immersed in Gd(III) solution (10 mL, pH = 7) with different initial concentrations (25, 50, 75, 100, 125, 150, 175 and 200 mg L^{-1}) for 12 hours.

2.4.4. Selectivity tests. 10 mg of PEI-CMC-IIS, PEI-CMC-NIIS and CMC-IIS was separately immersed into the coexisting system (Gd(III), Nd(III), Pr(III), Tb(III), and Fe(III), pH = 7) for 12 hours. The initial concentration of each metal ion was 50 mg L^{-1}. The distribution coefficients (K_d, mL g^{-1}), selectivity coefficient α, and relative selectivity coefficient β used to evaluate the adsorption selectivity of materials were calculated based on following equations:

$$K_d = \frac{(C_0 - C_e)V}{C_e M} \quad (2)$$

$$\alpha = \frac{K_{d1}}{K_{d2}} \quad (3)$$

$$\beta = \frac{\alpha_1}{\alpha_2} \quad (4)$$

where K_{d1} and K_{d2} is the distribution coefficients of materials to Gd(III) and interfering ions, respectively. α_1 and α_2 is the selectivity coefficients of PEI-CMC-IIS and PEI-CMC-NIIS, respectively.

2.4.5. Regenerability test. 10 mg of PEI-CMC-IIS was immersed into Gd(III) solution (10 mL, 50 mg L^{-1}, pH = 7) for 12 hours. After adsorption reaction, PEI-CMC-IIS was fetched from the solution then immersed into the eluent (1 M HCl) to remove the adsorbed Gd(III). 1 M of NaOH solution was used to activate the functionality of PEI-CMC-IIS. The entire adsorption–desorption experiments were conducted for five times.

3. Results and discussion

3.1. Morphology and structural characteristics

3.1.1. SEM analysis. As displayed in Fig. 2, the SEM images of PEI-CMC-IIS, PEI-CMC-NIIS and CMC-IIS adsorbents present the non-uniform and interconnected 3D network structure composed of numerous channels with diameters of around 1 μm. This 3D network structure depends on the sublimation of ice crystals with different mode during the freeze-drying process. Referring to previous reports, this structure could improve the surface area and greatly help the compressible property of adsorbents.[25,26] Fig. 2(a) and (b) reflect that the PEI-CMC-IIS and PEI-CMC-NIIS possess similar structure, suggesting the IIT causes no related change in morphology. Moreover, a large number of imprinting sites distributed on the wall of channels favor for the migration of cation to the functional groups, thus accelerating the adsorption process.

3.1.2. N_2 adsorption–desorption isotherms. Fig. 3 reveals the results of N_2 adsorption–desorption isotherms for PEI-CMC-IIS, PEI-CMC-NIIS and CMC-IIS adsorbents. It can be seen that all of them depict the type IV isotherm with long and narrow H3 hysteresis loop in the P/P_0 ranges of 0.6–1.0, 0.44–1.0 and 0.86–1.0, respectively, which indicates the presence of slit-shaped mesopores in adsorbents.[27–29] From the curves of pore size distribution, it can be found that the PEI-CMC-IIS, PEI-CMC-NIIS and CMC-IIS adsorbents own a large number of pores with diameter of below 5 nm. This may result from the sublimation of ice crystals with different size and mode during the freeze-drying process.[14] In addition, the peaks intensity below 5 nm of PEI-CMC-IIS and PEI-CMC-NIIS are much higher than that of CMC-IIS, suggesting that they have abundant mesopores than CMC-IIS, which may be attributed to secondary pores constructed by the spatial branched structure of PEI in PEI-CMC-IIS and PEI-CMC-NIIS. On account of the spatial branched structure of modified CMC by PEI, PEI-CMC-IIS (38.8 $m^2 g^{-1}$; 0.16 $cm^3 g^{-1}$) and PEI-CMC-NIIS (41.7 $m^2 g^{-1}$; 0.20 $cm^3 g^{-1}$) display the larger surface area and higher pore volume than CMC-IIS (24.3 $m^2 g^{-1}$; 0.04 $cm^3 g^{-1}$). Compared with PEI-CMC-NIIS, PEI-CMC-IIS shows a lower surface area and pore volume, which may be due to the existence of imprinting sites on the surface of PEI-CMC-IIS.[30]

3.1.3. TG analysis. Fig. 4 presents the TG curves of PEI-CMC-IIS, PEI-CMC-NIIS and CMC-IIS adsorbents. In all TG

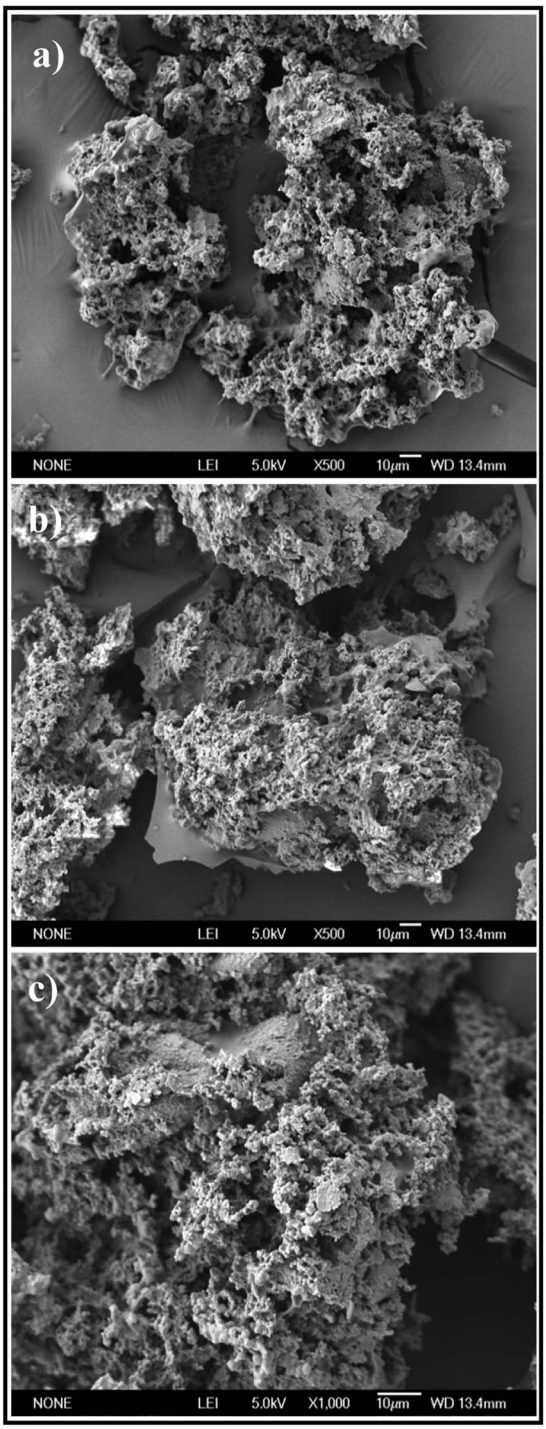

Fig. 2 SEM images of PEI-CMC-IIS (a), PEI-CMC-NIIS (b) and CMC-IIS (c).

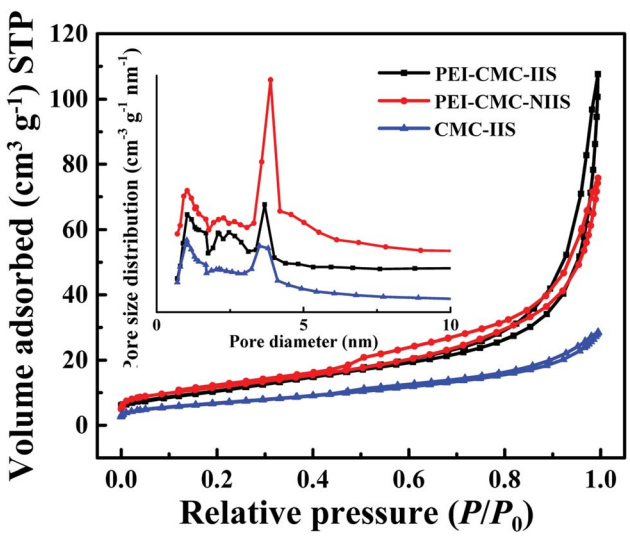

Fig. 3 N_2 adsorption–desorption isotherms and pore size distribution of PEI-CMC-IIS, PEI-CMC-NIIS and CMC-IIS.

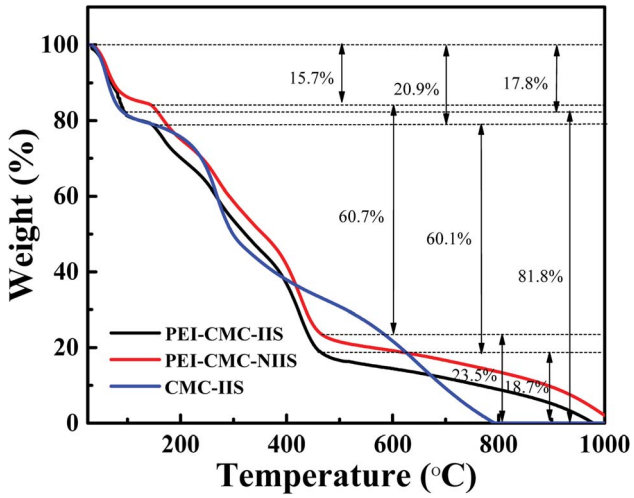

Fig. 4 TG curves of PEI-CMC-IIS, PEI-CMC-NIIS and CMC-IIS.

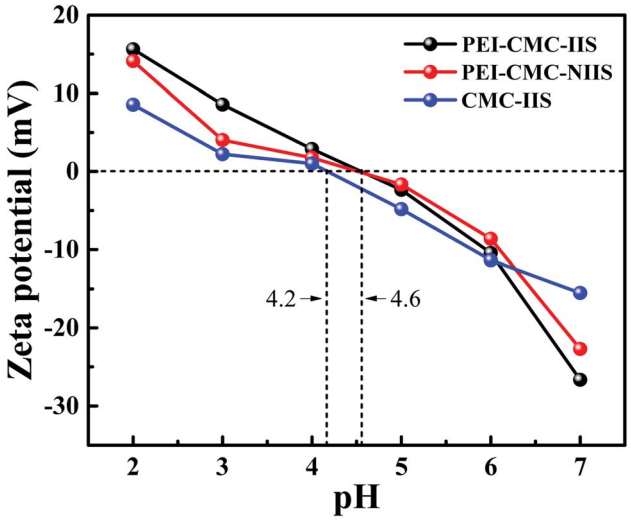

Fig. 6 Zeta potential of PEI-CMC-IIS, PEI-CMC-NIIS and CMC-IIS at different pH.

curves, occurred the characteristic temperature intervals in the range of 25–200 °C of weight loss relatives to the evaporation of physically adsorbed water.[31] Meanwhile, it can be observed that the CMC-IIS has a huge weight loss value of 81.8% in the temperature range of 200–800 °C, which could be associated with the depolymerization of polymer chains for CMC. By contrast, owing to the modification of CMC, the PEI-CMC-IIS and PEI-CMC-NIIS appear another two weight loss values in the temperature ranges of 200–450 °C and 450–1000 °C, which could be related to the depolymerization and decomposition of polymer backbones. This result evidences that the thermal stability of PEI-CMC-IIS and PEI-CMC-NIIS could be improved by functionalization of CMC by PEI.

3.1.4. FT-IR spectra and EA analysis. The FT-IR spectra of PEI-CMC-IIS, PEI-CMC-NIIS and CMC-IIS adsorbents in the range of 500–4000 cm^{-1} was characterized and the result was displayed in Fig. 5(a). Each adsorbent has a broad absorption peak at 3404 cm^{-1}, which belongs to the stretching vibration of $-NH_2$ and –OH groups. The characteristic peaks of 2936 and 2868 cm^{-1} are corresponding to the stretching vibration of C–H bond in the –CH, $-CH_2$ and $-CH_3$.[32] It is obvious observation that the intensity of –C=O absorption peak at 1710 cm^{-1} decreases in the PEI-CMC-IIS and PEI-CMC-NIIS, whereas the intensity of N–H bending vibration in $-NH_2$ at 1645 cm^{-1} increases in PEI-CMC-IIS and PEI-CMC-NIIS. This may be due to the occurrence of amination reaction between $-NH_2$ groups of PEI and –COOH groups of CMC.[33] Moreover, it can be clearly seen that the intensity of $-NH_2$ absorption peak greatly enhances in PEI-CMC-IIS and PEI-CMC-NIIS, which are due to the abundant $-NH_2$ groups in functionalized CMC. The FT-IR results reveal the successful functionality of CMC by PEI. Also are proved that PEI-CMC-IIS and PEI-CMC-NIIS almost have the same functional groups. As given in Fig. 5 (b), compared with CMC-IIS, PEI-CMC-IIS and PEI-CMC-NIIS present the increase in carbon and nitrogen contents, but the decrease in oxygen content for EA analysis, which further verifies the successful grafting of PEI on CMC.

3.1.5. Zeta potential analysis. Generally, there is essential relationship among the pH of solution, the species of cation in solution and the surface charge of the adsorbents.[34] In order to clearly understand the complicated adsorption mechanism,

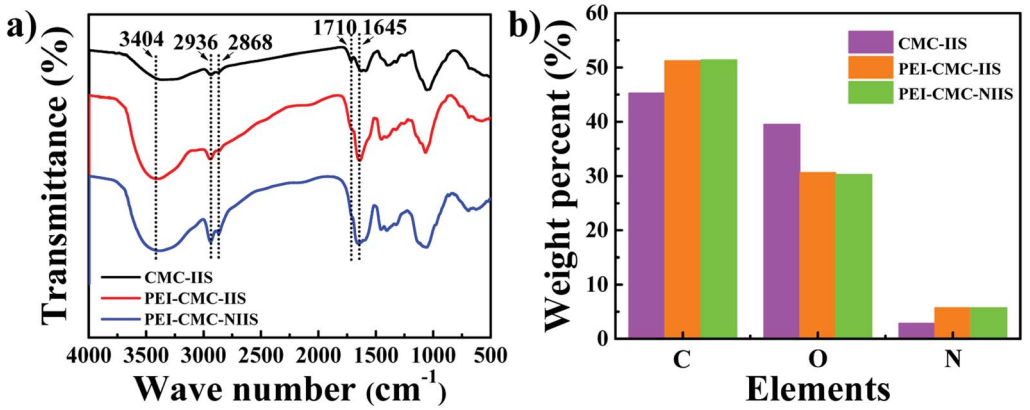

Fig. 5 FT-IR spectra (a) and EA (b) of PEI-CMC-IIS, PEI-CMC-NIIS and CMC-IIS.

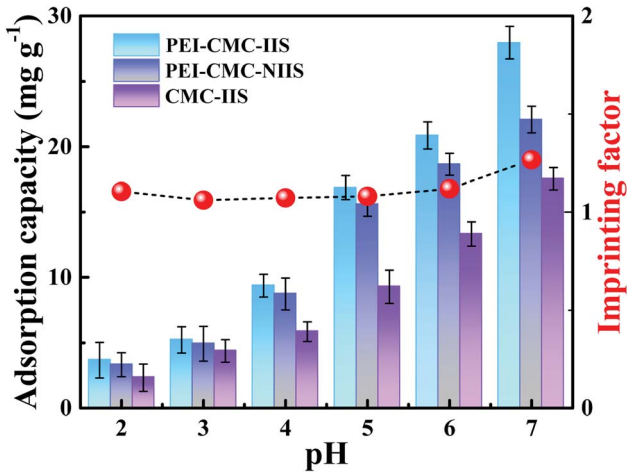

Fig. 7 Effect of pH on the adsorption capacity of Gd(III)overPEI-CMC-IIS, PEI-CMC-NIIS and CMC-IIS.

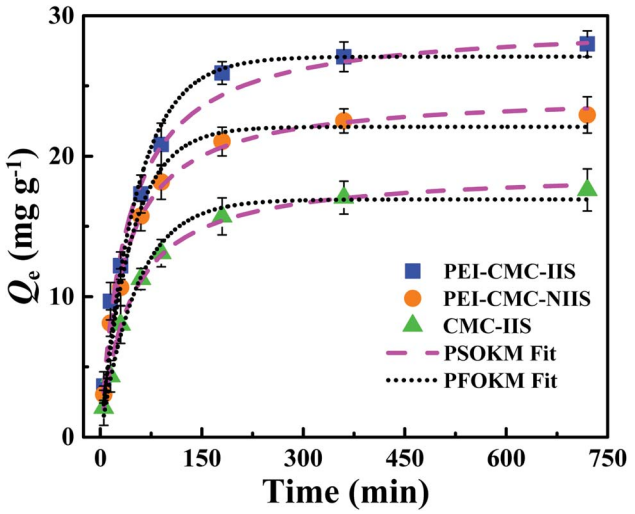

Fig. 8 Kinetics data and modeling of Gd(III) adsorption on PEI-CMC-IIS, PEI-CMC-NIIS and CMC-IIS.

a zeta potential test at different initial pH (2–7) was carried out, the result was shown in Fig. 6. It can be found that the surface potentials continuously decrease with the increase of pH and reach the minimum at pH 7 for PEI-CMC-IIS, PEI-CMC-NIIS and CMC-IIS. The points of zero charge for PEI-CMC-IIS, PEI-CMC-NIIS and CMC-IIS adsorbents are in the range of 4.2 to 4.6, identifying that the surface charges of materials are positive under acidic condition but negative close to neutral, which is associated with the protonation/deprotonation of the functional groups on the surface of adsorbents. In summary, the lowest surface negative charge at pH 7 helps the favorable adsorption condition towards Gd(III) from water.

3.2. Effect of initial solution pH on the adsorption capacity

To investigate the effect of solution pH on the adsorption capacity of adsorbents, the pH tests were conducted in the pH range of 2–7 due to the fact that Gd(III) could form the precipitate under alkaline conditions.[20] As observed from Fig. 7, the Gd(III) adsorption capacities for all of the adsorbents continually increase as the increasing pH and reach the maximum at pH = 7. This is possible due to that the species of cation in solution and the surface charge of functional groups on adsorbents change under different pH. In view of the result of zeta potential analysis, the protonated $-NH_3^+$ on the adsorbents and excessive H^+ in solution under acidic condition can prejudice the chelation with Gd(III). Under pH > 4, the $-NH_2$ on adsorbents gradually deprotonate with the increase of pH, the exposed lone pair of $-NH_2$ electrons are more conducive to the Gd(III) adsorption *via* chelation. In addition, PEI-CMC-IIS shows the best adsorption performance among three adsorbents, which proves that imprinting sites and the functionalization of CMC by PEI play a vital role in the adsorption process. It can be also observed that the imprinting factor (IF) is the highest at pH = 7, indicating that the separation ability of imprinted material is superior at this point. In consideration of the above all factors, the pH = 7 was chosen as the optimal pH in subsequent adsorption experiments.

3.3. Effect of contact time and adsorption kinetics

The kinetics assays of Gd(III) adsorption on PEI-CMC-IIS, PEI-CMC-NIIS and CMC-IIS were carried out to study the relationship between contact time and Gd(III) adsorption capacity. As illustrated in Fig. 8, the adsorption capacities rapidly increase with greater than 75% of the maximum adsorption capacities within 100 minutes then reach equilibrium within 4 hours. Due to the functionalizing of PEI, the as-prepared PEI-CMC-IIS and PEI-CMC-NIIS show the higher adsorption equilibrium capacities with respect to CMC-IIS. In addition, PEI-CMC-IIS possesses the superior adsorption equilibrium capacity than PEI-CMC-NIIS because of its adsorption specificity of imprinting sites. As a result, the pseudo-first-order and pseudo-second-order reaction kinetic models (PFOKM and PSOKM) were used to nonlinearly fit the kinetic data and elucidate the adsorption mechanism, which are expressed as follows:

$$Q_t = Q_1 - Q_1 e^{-k_1 t} \quad (5)$$

$$Q_t = \frac{k_2 Q_2^2 t}{1 + k_2 Q_2 t} \quad (6)$$

where k_1 (L min^{-1}) and k_2 (g mg^{-1} min^{-1}) are the rate constants, Q_1 and Q_2 (mg g^{-1}) are the theoretical adsorption capacity of the PFOKM and PSOKM, respectively. For the PSOKM, the initial adsorption rate h (mg g^{-1} min^{-1}) can be calculated by following equations:

$$h = k_2 Q_2^2 \quad (7)$$

The relevant parameters were summarized in Table 1. From the high correlation coefficient (R^2 > 0.99), it can be found that PSOKM better fits the adsorption kinetic data for all the adsorbents, suggesting that the chemical chelation plays a dominant rate-limiting role in the process of adsorption.[19] Also, it can be observed that the values of h follow the order: PEI-

Table 1 Kinetic parameters for Gd(III) adsorption on PEI-CMC-IIS, PEI-CMC-NIIS and CMC-IIS

		Pseudo-first-order kinetic model			Pseudo-second-order kinetic model			
Materials	$Q_{e,exp}$ (mg g^{-1})	$Q_{1,c}$ (mg g^{-1})	k_1 (L min^{-1})	R^2	$Q_{2,c}$ (mg g^{-1})	$k_2/10^{-2}$ (g mg^{-1} min^{-1})	h (mg g^{-1} min^{-1})	R^2
PEI-CMC-IIS	27.99	27.08	0.019	0.965	29.56	0.088	0.769	0.992
PEI-CMC-NIIS	22.94	22.10	0.022	0.980	24.50	0.121	0.728	0.994
CMC-IIS	17.59	16.77	0.023	0.988	20.90	0.143	0.623	0.996

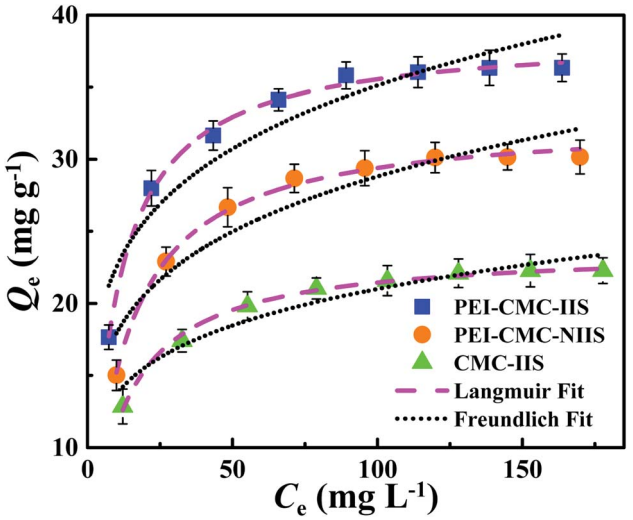

Fig. 9 Isotherm data and modeling of Gd(III) adsorption on PEI-CMC-IIS, PEI-CMC-NIIS and CMC-IIS.

CMC-IIS > PEI-CMC-NIIS > CMC-IIS, indicating that the functionalizing of PEI and lots of imprinting sites indeed potentialize adsorption kinetic property.

3.4. Effect of initial concentration and adsorption isotherms

The equilibrium experimental data of Gd(III) adsorption as a function of different initial Gd(III) concentration was obtained to find the maximum adsorption capacities of materials and the result was presented in Fig. 9. It can be found that the isotherms are characterized by initially continuous increase due to the excessive active sites on the surface of adsorbents at low Gd(III) concentration till equilibrium due to the complete occupancy of active sites by Gd(III) at high Gd(III) concentration. The maximum Gd(III) adsorption capacities follow the order: PEI-CMC-IIS > PEI-CMC-NIIS > CMC-IIS, indicating that lots of amino groups in PEI can indeed improve the adsorption capacity. The another important factor is that numerous imprinting sites located at the surface of adsorbents can help the adsorption of Gd(III) because of the specific spatial structure of imprinting cavities. In order to analyze the adsorption behavior, Langmuir and Freundlich isotherm models were nonlinearly fitted to experimental data, which are expressed as follows:

Table 3 K_d, α and β values of Nd(III), Pr(III), Tb(III), and Fe(III) with respect to Gd(III)

	PEI-CMC-IIS		PEI-CMC-NIIS		CMC-IIS		
Metal ions	K_d	α	K_d	α	K_d	α	β
Gd(III)	437.525	—	133.48	—	84.03	—	—
Nd(III)	87.098	5.02	139.71	0.96	81.67	1.03	5.26
Pr(III)	93.279	4.69	133.02	1.00	70.34	1.19	4.67
Tb(III)	140.62	3.11	181.03	0.74	127.98	0.66	4.22
Fe(III)	19.97	21.91	14.69	9.08	19.31	4.35	2.41

$$Q_e = \frac{K_L Q_m C_e}{1 + K_L C_e} \quad (8)$$

$$Q_e = K_F C_e^{1/n_F} \quad (9)$$

where Q_e and Q_m (mg g^{-1}) is the equilibrium adsorption capacity and saturated adsorption capacity, respectively. The K_L (L mg^{-1}) and K_F [(mg g^{-1}) (L mg^{-1})$^{1/n_F}$] are the Langmuir affinity constant and Freundlich constant, $1/n_F$ is heterogeneity factor.

The related parameters were enumerated in Table 2. For the all adsorbents, the higher correlation coefficients (R^2 > 0.99) corresponding to the Langmuir model indicate that the active sites are uniformly distributed on the surface of adsorbents.[14] Also can be observed that the monolayer chemical adsorption plays a leading role during the adsorption process. The maximum theoretical saturated adsorption capacities obtained from Langmuir model shows that the PEI-CMC-IIS has better potential for Gd(III) adsorption.

Table 2 Isotherm parameters for Gd(III) adsorption on PEI-CMC-IIS, PEI-CMC-NIIS and CMC-IIS

	Langmuir isotherm equation			Freundlich isotherm equation		
Materials	R^2	K_L (L mg^{-1})	Q_m (mg g^{-1})	R^2	K_F (mg g^{-1})	$1/n_F$
PEI-CMC-IIS	0.997	0.115	38.64	0.880	14.46	0.193
PEI-CMC-NIIS	0.996	0.086	32.79	0.873	11.15	0.206
CMC-IIS	0.995	0.092	23.78	0.916	8.934	0.186

Table 4 The comparison of REMs ions adsorption capacities with some previously reported adsorbents

Adsorbents	Target ion	pH	Adsorption capacity (mg g^{-1})	Selectivity	Reference
II-MAC	Dy(III)	7	23.3	Low	35
PAMAM@GTA–NH_2–MSF	Gd(III)	6	132	High	36
Mn_3O_4 nanoparticles	Gd(III)	5	12.6	Low	37
DCHCE	Gd(III)	5	2.02	Low	38
PEI-CMC-IIS	Gd(III)	7	38.65	High	This work

3.5. Selectivity test

Considering that the real waste solution (such as the waste solution of permanent magnet, fluorescent lamp and hard disk drives) usually contains several kinds of REMs ions, which leads to the complex selective separation for target ion due to their similar physicochemical properties, therefore, we selected Nd(III), Pr(III), Tb(III), and Fe(III) as interfered ions to investigate the selectivity of materials for target ion [Gd(III)]. For every adsorbent, a competitive adsorption among Nd(III), Pr(III), Tb(III), and Fe(III) for the same binding sites proceeds in

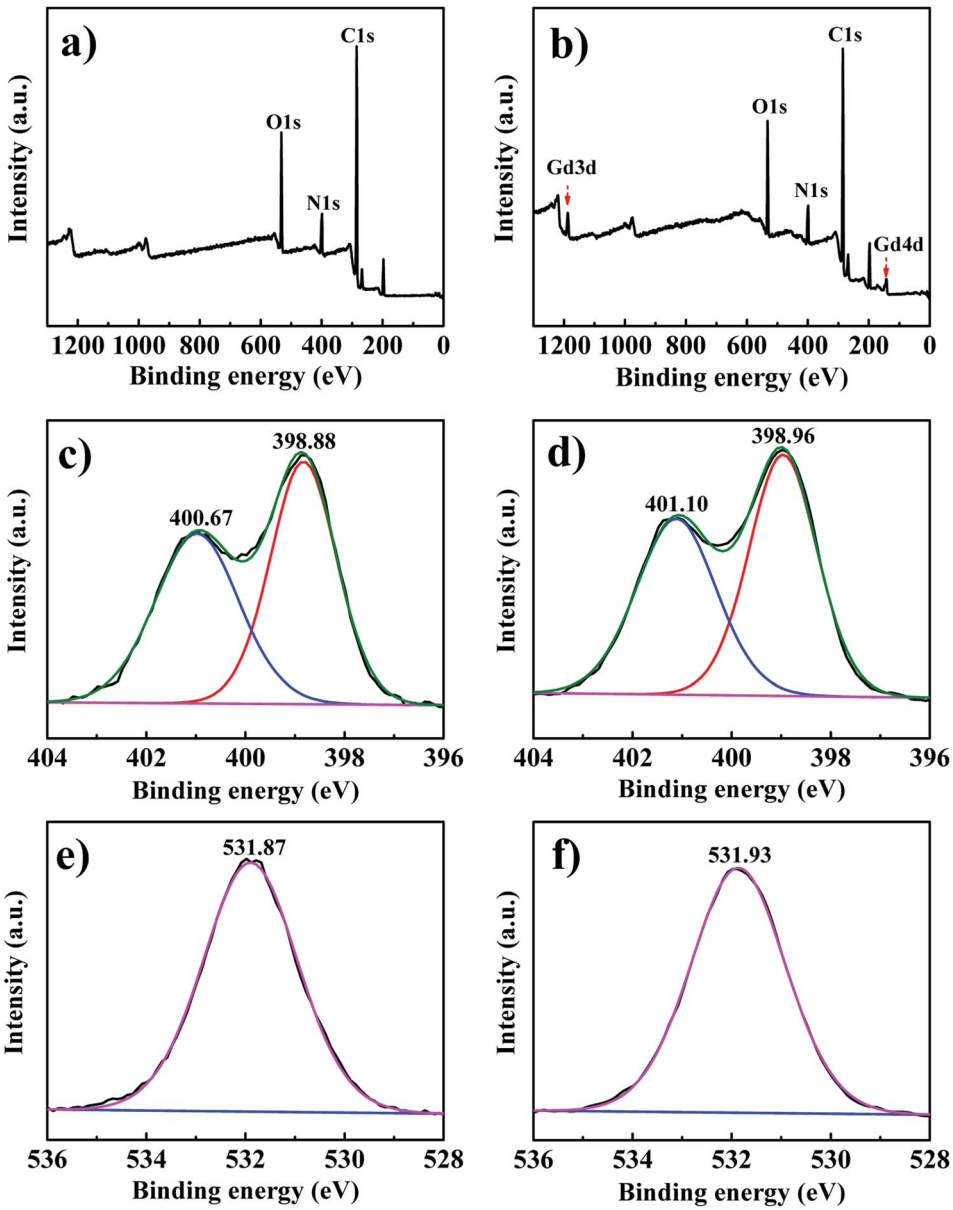

Fig. 10 Full XPS spectra of PEI-CMC-IIS before (a) and after (b) Gd(III) adsorption; XPS spectra of N 1s for PEI-CMC-IIS before (c) and after (d) Gd(III) adsorption; XPS spectra of O 1s for PEI-CMC-IIS before (e) and after (f) Gd(III) adsorption.

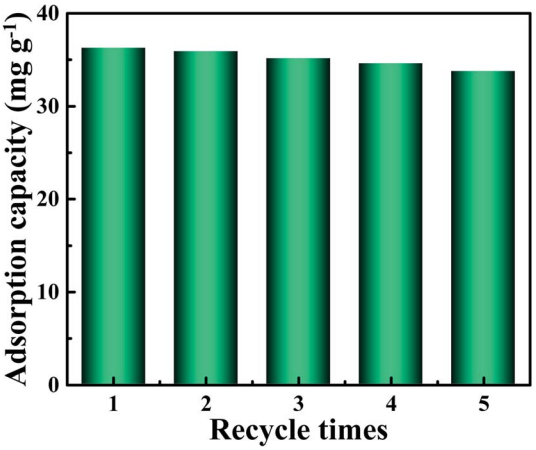

Fig. 11 Results of five consecutive adsorption–desorption cycles for PEI-CMC-IIS.

a coexisting ions system. The results of selective tests were summarized in Table 3. It is found that the K_d value of PEI-CMC-IIS for Gd(III) is the highest, that is 5.0, 4.7, 3.1 and 21.9 times higher than Nd(III), Pr(III), Tb(III) and Fe(III), respectively. The β value of PEI-CMC-IIS for Gd(III)/Nd(III), Gd(III)/Pr(III), Gd(III)/Tb(III), and Gd(III)/Fe(III) is 5.2, 4.6, 4.2 and 2.4 times greater than that of PEI-CMC-NIIS, respectively. These suggest that the affinity of PEI-CMC-IIS with Gd(III) is much higher than that of PEI-CMC-NIIS. This phenomenon further verifies that imprinting cavities with special spatial structure can indeed achieve the selective adsorption for target ion Gd(III).

3.6. Comparison with other adsorbents

Considering the factors such as adsorption capacity and selectivity are the most direct indexes to assess the practicability of adsorbent, the comparison with other adsorbents used to adsorb REM ions was carried out.[35–38] As summarized in Table 4, it can be observed that the adsorption capacity of PEI-CMC-IIS is not the highest, but PEI-CMC-IIS simultaneously possesses comparable adsorption capacity and excellent selectivity under neutral conditions, which is superior to other adsorbents in some way. Moreover, the main advantages of PEI-CMC-IIS are the cost-effective design, good stability, easy separation, pollution-free for the treated water, satisfactory adsorption capacity and selectivity.

3.7. Adsorption mechanism

XPS was used to analyze the interaction mechanism between PEI-CMC-IIS and Gd(III), the result is shown in Fig. 10. It can be clearly observed from the full XPS spectra of PEI-CMC-IIS that two new peaks of Gd 3d and Gd 4d at about 1189.7 eV and 143.1 eV are presented after Gd(III) adsorption. This result directly proves the adsorption of Gd(III) on PEI-CMC-IIS. In the high resolution of XPS spectra of N 1s, the two peaks of 400.67 eV and 398.88 eV corresponding to the N–C and C=N bonds in PEI-CMC-IIS shift to higher binding energy (401.10 eV and 398.96 eV) after Gd(III) adsorption, which is attributed to the chelation between the Gd(III) and N-containing functional groups in PEI-CMC-IIS. Furthermore, the binding energy of C–O increases from 531.87 eV to 531.93 eV after Gd(III) adsorption, suggesting that –OH groups are involved in the chelation with Gd(III). Based on the above discussions, the adsorption mechanism of PEI-CMC-IIS is mainly summarized as following:[1] The chelation between O/N-containing functional groups on PEI-CMC-IIS and Gd(III);[2] the unique spatial structure of imprinting cavities achieves the selective adsorption in size for Gd(III).

3.8. Reusability tests

In order to verify the practical application value of PEI-CMC-IIS, the repetitive adsorption–desorption tests were conducted and illustrated in Fig. 11. It can be observed that the adsorption performance of PEI-CMC-IIS shows a slightly downturn after 5 times recycle, but still keeps around 90% maximum adsorption capacity. Although the incomplete desorption of adsorbed Gd(III) and the destruction of active sites may affect the adsorption performance, the as-fabricated PEI-CMC-IIS adsorbent still has a promising application prospect in the selective adsorption of Gd(III).

4. Conclusion

In this work, a novel adsorbent (PEI-CMC-IIS) was fabricated by a simple polymerization–lyophilization method for the effective and selective adsorption of Gd(III) from aqueous solution. The thermal stability and adsorption properties were proved *via* a series of characterization. Systematic adsorption tests show that PEI-CMC-IIS has a maximum adsorption capacity of 38.64 mg g^{-1} under pH = 7. The kinetic studies prove that adsorption specificity of imprinting sites can improve adsorption kinetic properties and capacity. The isotherm studies indicate that the graft of PEI on CMC can improve the adsorption capacity of PEI-CMC-IIS. Fitting results of kinetic and isotherm data confirm that the adsorption mechanism of PEI-CMC-IIS to Gd(III) pertains to monolayer chemical adsorption. The selectivity tests suggest that PEI-CMC-IIS can achieve the selective adsorption for Gd(III). The reusability experiments affirm that PEI-CMC-IIS can be as a stable and reliable adsorbent.

Conflicts of interest

There are no conflicts to declare.

Acknowledgements

We would like to acknowledge the National Natural Science Foundation of China (31971616 and 32130073), the Science and Technology Development Project of Jilin Province (YDZJ202101ZYTS070), and the Science and Technology Research Project of the Department of Education of Jilin Province (JJKH20200039KJ).

References

1 L. Zhang, C. Wang and R. Yang, Novel environment-friendly magnetic bentonite nanomaterials functionalized by carboxymethyl chitosan and 1-(2-pyridinylazo)-2-naphthalene for adsorption of Sc (III), *Appl. Surf. Sci.*, 2021, **566**, 150644.

2 Y. Lee, Y. Ren, M. Cui, J. Ma, Z. Han, O. Kwon, J. Ko and J. Khim, Rare earth real wastewater treatment by pilot scale using new concept continuous treatment process, *Chemosphere*, 2021, **279**, 130523.

3 F. Nkinahamira, A. Alsbaiee and Y. Wang, Recovery and purification of rare earth elements from wastewater and sludge using a porous magnetic composite of β-cyclodextrin and silica doped with PC88A, *Sep. Purif. Technol.*, 2021, **266**, 118589.

4 T. H. Darrah, J. J. Prutsman-Pfeiffer, R. J. Poreda, M. E. Campbell, P. V. Hauschka and R. E. Hannigan, Incorporation of excess gadolinium into human bone from medical contrast agents, *Metallomics*, 2009, **1**, 479–488.

5 Y. Zhang, T. Bian, R. Jiang, Y. Zhang, X. Zheng and Z. Li, Bionic chitosan-carbon imprinted aerogel for high selective recovery of Gd(III) from end-of-life rare earth productions, *J. Hazard. Mater.*, 2021, **407**, 124347.

6 E. Liu, X. Lin and D. Zhang, Ionic imprinted CNTs-chitosan hybrid sponge with 3D network structure for selective and effective adsorption of Gd (III), *Sep. Purif. Technol.*, 2021, **269**, 118792.

7 M. Zhang, Z. Dong and F. Hao, Ultrahigh and selective adsorption of Au (III) by rich sulfur and nitrogen-bearing cellulose microspheres and their applications in gold recovery from gold slag leaching solution, *Sep. Purif. Technol.*, 2021, **274**, 119016.

8 J. Liu, Y. Chen and S. Jiang, Rapid removal of Cr (III) from high-salinity wastewater by cellulose-g-poly-(acrylamide-co-sulfonic acid) polymeric bio-adsorbent, *Carbohyd. Polym.*, 2021, **270**, 118356.

9 S. S. Zamil, M. H. Choi and J. H. Song, Enhanced biosorption of mercury (II) and cadmium (II) by cold-induced hydrophobic exobiopolymer secreted from the psychrotroph Pseudomonas fluorescens BM07, *Appl. Microbiol. Biot.*, 2008, **80**, 531–544.

10 H. Wu, T. Kawamura and S. Kim, Adsorption and separation behaviors of Y(III) and Sr(II) in acid solution by a porous silica based adsorbent, *Nucl. Eng. Technol.*, 2021, **53**, 3352–3358.

11 L. Zhang, C. Wang and R. Yang, Novel environment-friendly magnetic bentonite nanomaterials functionalized by carboxymethyl chitosan and 1-(2-pyridinylazo)-2-naphthalene for adsorption of Sc (III), *Appl. Surf. Sci.*, 2021, **566**, 150644.

12 H. Javadian, M. Ruiz and M. Taghavi, Synthesis of magnetic CMC bionanocomposite containing a novel biodegradable nanoporous polyamide selectively synthesized in ionic liquid as green media: Investigation on Nd^{3+}, Tb^{3+}, and Dy^{3+} rare earth elements adsorption, *J. Mol. Liq.*, 2020, **308**, 113017.

13 H. Shehzad, Z. H. Farooqi and E. Ahmed, Fabrication of a novel hybrid biocomposite based on amino-thiocarbamate derivative of alginate/carboxymethyl chitosan/TiO_2 for Ni (II) recovery, *Int. J. Boil. Macromol.*, 2020, **152**, 380–392.

14 Y. Zhang, T. Bian and R. Jiang, Bionic chitosan-carbon imprinted aerogel for high selective recovery of Gd(III) from end-of-life rare earth productions, *J. Hazard. Mater.*, 2021, **407**, 124347.

15 X. Zheng, Y. Zhang and T. Bian, Selective extraction of gadolinium using free-standing imprinted mesoporous carboxymethyl chitosan films with high capacity, *Cellulose*, 2019, **26**, 1209–1219.

16 M. Chen and N. P. Hankins, Interaction among branched polyethylenimine (PEI), sodium dodecyl sulfate (SDS) and metal cations during copper recovery from water using polymer-surfactant aggregates, *J. Water Process Eng.*, 2020, **34**, 101170.

17 G. Sun, L. Zhou and X. Tang, In situ formed magnetic chitosan nanoparticles functionalized with polyethylenimine for effective U (VI) sorption, *J. Radioanal. Nucl. Ch.*, 2020, **325**, 595–604.

18 F. Zhao, Z. Yang and Z. Wei, Polyethylenimine-modified chitosan materials for the recovery of La(III) from leachates of bauxite residue, *Chem. Eng. J.*, 2020, **388**, 124307.

19 J. K. Bediako, S. Lin and A. K. Sarkar, Benignly-fabricated crosslinked polyethylenimine/calcium-alginate fibers as high-performance adsorbents for effective recovery of gold, *J. Clean. Prod.*, 2020, **252**, 119389.

20 W. Yin, L. Liu and S. Tang, Facile synthesis of triazole and carboxyl-functionalized cellulose-based adsorbent via click chemistry strategy for efficient Gd (III) removal, *Cellulose*, 2019, **26**, 7107–7123.

21 N. H. Elsayed, R. A. S. Alatawi and M. Monier, Amidoxime modified chitosan based ion-imprinted polymer for selective removal of uranyl ions, *Carbohyd. Polym.*, 2021, **256**, 117509.

22 W. Ma, X. Du and M. Liu, A conductive chlorine ion-imprinted polymer threaded in metal-organic frameworks for electrochemically selective separation of chloride ions, *Chem. Eng. J.*, 2021, **412**, 128576.

23 X. Zhang, X. Ou and J. Zhang, Smart ion imprinted polymer for selective adsorption of Ru (III) and simultaneously waste sample being transformed as a catalyst, *J. Hazard. Mater.*, 2021, **417**, 126072.

24 X. Liu, Y. Mo, X. Liu, R. Guo, Y. Zhang, W. Xue, Y. Zhang, C. Wang and S. Ramakrishna, Synthesis, characterisation and preliminary investigation of the haemocompatibility of polyethyleneimine-grafted carboxymethyl chitosan for gene delivery, *Mat. Sci. Eng. C*, 2016, **62**, 173–182.

25 R. Bai, F. Yang, Y. Zhang, Z. Zhao, Q. Liao, P. Chen, P. Zhao, W. Guo and C. Cai, Preparation of elastic diglycolamic-acid modified chitosan sponges and their application to

recycling of rare-earth from waste phosphor powder, *Carbohyd. Polym.*, 2018, **190**, 255–261.

26 L. Mo, H. Pang, Y. Tan, S. Zhang and J. Li, 3D multi-wall perforated nanocellulose-based polyethylenimine aerogels for ultrahigh efficient and reversible removal of Cu(II) ions from water, *Chem. Eng. J.*, 2019, **378**, 122157.

27 K. Li, Q. Gao, G. Yadavalli, X. Shen, H. W. Lei, B. Han and K. S. Xia, Selective adsorption of Gd^{3+} on a magnetically retrievable imprinted chitosan/carbon nanotube composite with high capacity, *ACS Appl. Mater. Interfaces*, 2015, **7**, 21047–21055.

28 E. Liu, X. Lin, Y. Hong, L. Yang, B. Luo, W. Shi and J. Shi, Rational copolymerization strategy engineered C self-doped g-C_3N_4 for efficient and robust solar photocatalytic H_2 evolution, *Renewable Energy*, 2021, **178**, 757–765.

29 Y. Hong, L. Wang, E. Liu, J. Chen, Z. Wang, S. Zhang, X. Lin, X. Duan and J. Shi, A curly architectured graphitic carbon nitride (g-C_3N_4) towards efficient visible-light photocatalytic H_2 evolution, *Inorg. Chem. Front.*, 2020, **7**, 347–355.

30 X. Zheng, E. Liu, F. Zhang, Y. Yan and J. Pan, Efficient adsorption and separation of dysprosium from NdFeB magnets in acidic system by ion imprinted mesoporous silica sealed in dialysis bag, *Green Chem.*, 2016, **18**, 5031–5040.

31 B. Chen, H. Zhao and S. Chen, A magnetically recyclable chitosan composite adsorbent functionalized with EDTA for simultaneous capture of anionic dye and heavy metals in complex wastewater, *Chem. Eng. J.*, 2019, **356**, 69–80.

32 D. Zhang, L. Wang, H. Zeng, P. Yan, J. Nie, V. K. Sharma and C. Wang, A three-dimensional macroporous network structured chitosan/cellulose biocomposite sponge for rapid and selective removal of mercury(II) ions from aqueous solution, *Chem. Eng. J.*, 2019, **363**, 192–202.

33 Y. Wang, D. Wu and Q. Wei, Rapid removal of Pb (II) from aqueous solution using branched polyethylenimine enhanced magnetic carboxymethyl chitosan optimized with response surface methodology, *Sci. Rep.*, 2017, **7**, 1–11.

34 A. Alshameri, H. He and J. Zhu, Adsorption of ammonium by different natural clay minerals: characterization, kinetics and adsorption isotherms, *Appl. Clay Sci.*, 2018, **159**, 83–93.

35 E. L. Liu, X. C. Xu, X. D. Zheng, F. S. Zhang, E. X. Liu and C. X. Li, An ion imprinted macroporous chitosan membrane for efficiently selective adsorption of dysprosium, *Sep. Purif. Technol.*, 2017, **189**, 288–295.

36 Y. R. Lee, S. Q. Zhang, K. Yu, J. Choi and W. S. Ahn, Poly(amidoamine) dendrimer immobilized on mesoporous silica foam (MSF) and fibrous nano-silica KCC-1 for Gd^{3+} adsorption in water, *Chem. Eng. J.*, 2019, **378**, 122133.

37 M. A. Sayed, A. I. Helal and S. M. Abdelwahab, Sorption and possible preconcentration of europium and gadolinium ions from aqueous solutions by Mn_3O_4 nanoparticles, *Chem. Pap.*, 2020, **74**, 619–630.

38 P. Sappidi, A. Boda, S. M. Ali and J. K. Singh, Adsorption of gadolinium (Gd^{3+}) ions on the dibenzo crown ether (DBCE) and dicyclo hexano crown ether (DCHCE) grafted on the polystyrene surface: Insights from all atom molecular dynamics simulations and experiments, *J. Phys. Chem. C*, 2019, **123**, 12276–12285.